Geoderma 444 (2024) 116858

Contents lists available at ScienceDirect

Geoderma

journal homepage: www.elsevier.com/locate/geoderma

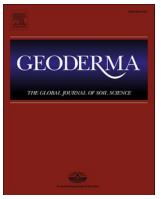

Fire simulation effects on the transformation of iron minerals in alpine soils

Sara Negri [a,*], Beatrice Giannetta [a,b], Jessica Till [c], Danilo Oliveira de Souza [4], Daniel Said-Pullicino [a], Eleonora Bonifacio [a]

[a] University of Torino, Department of Agricultural, Forest and Food Sciences, Largo Braccini 2, 10095 Grugliasco, Italy
[b] University of Verona, Department of Biotechnology, Strada Le Grazie 15, 37134 Verona, Italy
[c] Institute for Rock Magnetism, Department of Earth and Environmental Sciences, 150 John T. Tate Hall, 116 Church St. SE, Minneapolis, MN 55455, USA
[4] ELETTRA Sincrotrone Trieste S.C.p.A, S.S. 14 Km 163.5, 34149 Basovizza, Trieste, Italy

ARTICLE INFO

Handling Editor: K. Vancampenhout

Keywords:
Fe oxides
Forest soils
Organic matter
Thermal treatment
X-ray absorption spectroscopy
Magnetism

ABSTRACT

Heat-induced changes in topsoil iron (Fe) species triggered by the relatively low temperatures (Ts) produced by wildfires (200–300 °C) have not been fully elucidated. Changes in the chemistry of Fe minerals can produce cascading impacts on the environment, and the resulting aftermath may be exacerbated in erosion-prone alpine soils. The aim of this study was to determine - at environmentally realistic conditions - changes in the composition and crystallinity of Fe species, and the dispersible organic matter (OM) pool (evaluated by the pyrophosphate extraction), as a function of rising Ts, native Fe phases and OM in alpine soils. Multiple techniques were employed, including X-ray diffraction (XRD), field-emission scanning electron microscopy (FE-SEM), magnetic measurements and Fe K-edge X-ray absorption spectroscopy (XAS). The results demonstrated the dominance of poorly crystalline Fe phases at 300 °C. At the same T, we observed the partial conversion of maghemite to hematite (supporting the involvement of oxidative processes) and, in the presence of high organic carbon (OC) contents, an enrichment in magnetic minerals (suggesting the onset of reducing conditions). The heat-induced modifications in Fe species and organic compounds did not promote the stabilization of the remaining OM, highlighting the weak nature of soil organo-mineral associations in an after-fire scenario. These phenomena can be further aggravated in case of the steep terrain that characterize alpine soils.

1. Introduction

Fire has been shaping landscapes all over the world since the late Devonian (Glasspool et al., 2015), long exposing soils to its effects. Increase in wildfires size, frequency and intensity are occurring globally due to climate-change (Bowman et al., 2009), and projections for future years forecast even more disruptive events (Jolly et al., 2015).

The occurrence of fire can induce substantial modifications in soils (Certini, 2005). Soil temperatures (Ts) as high as 300–700 °C have been recorded at the soil surface during the burning of shrubland vegetation (Gimeno-García et al., 2004). In wildfires, the extent of soil heating can vary between Ts < 250 °C for low severity fires, around 450 °C for moderate severity fires, and up to 650 °C in high severity fires (Janzen and Tobin-Janzen, 2008). Typically, only the topsoils experience consistent heat transfer due to the low thermal conductivity of the soil matrix (DeBano et al., 1998). The Ts rarely exceed 100 °C below the first 2 cm (Badía-Villas et al., 2014) or 5 cm (Merino et al., 2018) from the mineral soil surface. Still, the effects can be impactful since the areas exposed to fire occurrence are extremely vast.

Soil organic matter (OM) starts undergoing significant biochemical transformations at 150–200 °C (Merino et al., 2018). The majority of soil minerals are only affected by Ts higher than 500 °C (Reynard-Callanan et al., 2010; Ulery et al., 1996), which are not typically experienced below-ground (Näthe et al., 2017). Iron (Fe) oxyhydroxides (hereafter referred to as Fe oxides) are among the few mineral phases to be affected by milder heating (Burton et al., 2019).

As evidence of their sensitivity to heating, wildfire-affected areas have been found to display a notable increase in surface magnetism

Abbreviations: BSE, back-scattered electron; DCB, Na-Dithionite-citrate-bicarbonate; EXAFS, Extended X-ray absorption fine-structure; FC, field-cooling; Fe, iron; FE-SEM, field-emission scanning electron microscopy; H_C, coercitivity; M_R, remanent magnetization; M_S, saturation magnetization; OC, organic carbon; OM, organic matter; OXA, ammonium oxalate; PYRO, sodium pyrophosphate; RT, room temperature; SE, secondary electrons; SIRM, saturation isothermal remanence; T, temperature; XANES, X-ray absorption near-edge spectroscopy; XAS, X-ray absorption spectroscopy; XRD, X-Ray diffraction; ZFC, zero-field-cooling.

* Corresponding author.
E-mail address: sara.negri@unito.it (S. Negri).

https://doi.org/10.1016/j.geoderma.2024.116858
Received 1 March 2023; Received in revised form 29 January 2024; Accepted 12 March 2024

(Jordanova et al., 2019), and mineralogy in heat/fire-impacted soils has gained much attention as a promising marker of soil burn severity. Some authors explain this phenomenon as a heat-mediated increase in low-coercitivity components (Clement et al., 2011). Others attribute magnetism mainly to a combustion-induced mass-loss effect, with concentration of magnetic phases rather than neo-formation of magnetic minerals (Jordanova et al., 2019; Till et al., 2021).

Thermal alteration of isolated soil Fe oxides has been studied since the 1980 s, revealing a multiplicity of possible speciation dynamics according to composition, grain size and morphology of the starting mineral particles or, conversely, the convergence of many Fe phases to the same final product. For example, engineered mineral mixtures of ferrihydrite and goethite have been reported to experience minor changes until 200 °C (Johnston et al., 2019), and transition to maghemite at 400 °C (Cornell and Schwertmann, 2003). Magnetite, on the other hand, can result upon heating of lepidocrocite, hematite or ferrihydrite (Cornell and Schwertmann, 2003).

The content and composition of OM could influence Fe speciation in soil during burning (Till and Nowaczyk, 2018) as high-temperature induced electron shuttling from OM to electron acceptors may not always involve O_2 (Schwertmann, 1988; Yang et al., 2016). This is due to a fast consumption of O_2 with respect to its limited diffusion, further hindered by consistent heat-induced water evaporation (Jeleńska et al., 2010). Consequently, Fe(III) in Fe species like hematite may act as an electron acceptor and be reduced (Jozwiak et al., 2007).

Abundance and composition of Fe species are known to drive organic carbon (OC) persistence in soils, primarily due to their high specific surface area and affinity for binding organic moieties (Czimczik and Masiello, 2007; Kaiser and Guggenberger, 2007; Wagai and Mayer, 2007). Hence, soil Fe phase transformations might lead to sharp modifications in C cycling due to altered organo-mineral interactions (Buettner et al., 2014). These dynamics may be exacerbated in alpine and mountain soils, where after-fire intrinsic fragility is derived from loss of physical integrity due to steep slopes and exposure to large precipitation events (Smith et al., 2011).

The uncertainty related to Fe speciation dynamics in fire-affected soils is favored by the complex nature of these systems, where pedogenic Fe oxides of multiple crystalline degrees appear in association with a wide spectrum of organic compounds and mineral phases. Few techniques allow proper identification of soil Fe species and associated OM at the atomic-scale, especially when looking at small variations induced by a relatively moderate heating treatment that, still, corresponds to the temperature thresholds realistically encountered in soils during wildfires.

Therefore, the aims of this study were to: i) verify whether the thermal transformations soil Fe oxides were primarily driven by starting mineralogy and OM content and composition; ii) elucidate the evolution of the OM pool towards which Fe phases display the highest affinity.

2. Materials and methods

2.1. Soil samples and heating treatment

A set of 18 soil samples belonging to an ecological region that has recently suffered from uncommonly disruptive fire seasons was employed for the study (Rita et al., 2020). These soils are representative of the North-Western Italian alpine relief for degree of pedogenesis, parent material and forest cover (hence soil OM quality), and a detailed site characterization is available in Supporting Information (Table S1 and Figure S1). They were classified as Regosols and Cambisols (WRB, 2015), displaying little development. They all belong to the geological complex of Schists with Green Stones (Servizio Geologico d'Italia, 2009), but differ in lithology, i.e., mainly ophiolitic outcrops and calcschists, canopy cover, i.e., *Fagus sylvatica* L. (BEECH subset, 10 BE samples) and *Pinus sylvestris* L. (PINE subset, 8 PI samples), and present variable OC contents (ranging from 13.2 g kg^{-1} to 97.1 g kg^{-1}, Table S2). The pH values of soil samples range from 4.0 to 7.9 (Table S2). The sampled sites did not experience burning in the last 10 years.

After removing litter and organic horizons, the upper 5 cm of the A horizon were collected (approximately 1 kg of soil). The samples were air-dried, sieved (2 mm), lab-heated and characterized in a previous work (Negri et al., 2021). Briefly, heating was performed in a furnace (Memmert GmbH + Co. KG UF260, Schwabach, Germany) for 30 min at increasing Ts (from 25 °C to 300 °C). Similar lab-heating experiments are widely used to mimic the effects of fire on soils (Araya et al., 2017; Badía-Villas et al., 2014; Merino et al., 2018) and, despite being a simplified system, they represent a good compromise that allows to rule out the complications posed by field natural variability. The alterations simulated in this study are expected to represent those occurring in the top 2 cm of mineral soil, as testified by studies carried out in fire-affected areas (Jordanova et al., 2019). In our sites, the steepness of the slopes (Table S1) induces the formation of thin organic horizons, that would be consumed in a fire event, exposing the underlying surface of the mineral soil. Heating time was set to 30 min in agreement with recent studies (Araya et al., 2017, 2016; Varela et al., 2010).

For the current experiment, samples kept at room-temperature (RT, 25 °C) were compared with samples heated at Ts of 200 and 300 °C (to test the influence of heating Ts and canopy cover). The T-thresholds were selected according to three main criteria: 1) correspondence with Ts widely experienced in fire-affected topsoils (Janzen and Tobin-Janzen, 2008); 2) T-range favorable for the induction of Fe speciation; 3) occurrence of major variations in organo-mineral associations detected exactly at 200 and 300 °C in our previous investigation (Negri et al., 2021).

2.2. Wet chemistry

Na-Dithionite-citrate-bicarbonate (DCB) was used to quantify total pedogenic Fe oxides (Mehra and Jackson, 1958), while ammonium oxalate solution in the dark (OXA) was employed to assess the contribution of poorly ordered Fe oxides (Schwertmann, 1964). The OM-bound Fe pool was isolated with a sodium pyrophosphate solution (PYRO) (Loeppert, 1996). Fe concentrations in the extracts were quantified by atomic absorption spectrometry, AAS (PerkinElmer AAnalyst 400, Norwalk, CT, USA). The different Fe pools are henceforth addressed as Fe_{DCB}, Fe_{OXA} and Fe_{PYRO}, respectively.

The OM present in the PYRO-extracts was also characterized, knowing that it comprises all the dispersible OM pools, i.e. free, water soluble, in organo-metallic complexes and bound to polymeric metal phases and small sized minerals (Kögel-Knabner et al., 2008). The OC concentrations in the 0.45 μm filtered PYRO extractants (OC_{PYRO}) were determined by Pt-catalyzed high T combustion (650 °C) followed by infrared CO_2 detection (VarioTOC, Elementar, Hanau, Germany). Optical properties of the PYRO-extracts were inspected (Helios UV–Vis spectrophotometer, Thermo Electron, Massachusetts, USA) to derive Specific UV absorbance (SUVA) and the E2:E3 ratio (proxy for aromaticity and molecular size of the dissolved OM, respectively) (Peuravuori and Pihlaja, 1997; Weishaar et al., 2003). Method blanks were analyzed in parallel with the samples.

The extractions were carried out on all the samples, while additional instrumental techniques (sections 2.3, 2.4, 2.5) were applied for selected specimens only. These soils were chosen to represent different parent material (BE4 and PI7 developed on schist, while BE10 and PI5 developed on serpentine), forest cover (BEECH *vs.* PINE), and presented a wide variability in OC contents: 31.3 g kg^{-1} in BE4, 39.7 g kg^{-1} in BE10, 76.2 g kg^{-1} in PI5, 69.3 g kg^{-1} in PI7 (for complete data see Table S2).

2.3. Microscopy analyses and X-ray diffraction

Electron microscopy is commonly used to observe the dimensions and crystal habitus of Fe oxides (LaGrow et al., 2019; Sayed and

Polshettiwar, 2015), and here it was used to inspect the morphology and elemental composition of Fe-rich particles. A field-emission scanning electron microscopy (FE-SEM, TESCAN S9000G) was employed, with an energy dispersive spectrometer (EDS, Oxford detector). A small amount (~30 mg) of powdered sample was mounted on stubs with carbon conductive tape and sputtered with a thin (25 nm) film of gold. The samples were examined at an accelerating voltage of 10–20 kV both in back-scattered electron (BSE) and secondary electrons (SE) emission mode. Several (ca. 5) regions of interest were selected for each sample, primarily focusing on areas with greater BSE intensity. The elemental maps derived by the EDS probe were acquired at dwell time of 10–50 μs, and processed with the AZTEC software.

Soil mineralogy was characterized in finely ground randomly oriented mounts by XRD using a Philips PW 1710 diffractometer (40 kV, 20 mA, Co-Kα radiation and graphite monochromator). Scans were acquired from 2° to 50° 2θ at a speed of 1° 2θ min^{-1}. Background subtraction and data smoothing was performed with PowderX software (Dong, 1999). Phase identification was carried out using the International Centre for Diffraction Data (ICDD) database.

2.4. Magnetic measurements

Small amounts (100 mg) of finely ground soil samples were packed into gelatin capsules with quartz wool for hysteresis and low-T magnetic measurements (loss-on-ignition, LOI, values in Table S3). Hysteresis loops were measured on a vibrating sample magnetometer at RT up to a maximum field of 1 T to account for saturation magnetization (M_S), saturation remanent magnetization (M_R) and coercitivity (H_C), after applying an appropriate fitting method for high-field slope correction (Jackson and Solheid, 2010). Low-T magnetic properties were measured on two selected samples (BE4 and PI5), and additional information on phase transitions were derived by low-T magnetization using a SQUID magnetometer (MPMS, Quantum Design, San Diego, CA, United states). Low-T procedures included measuring a saturation isothermal remanence (SIRM) imparted at 20 °K on warming to 300 °K after either field-cooling (FC) or zero-field-cooling (ZFC), as well as low-T cycling of RT SIRM, known as the FC-ZFC-LTSIRM-RTSIRM-LTD protocol (Bilardello and Jackson, 2013). All remanence and susceptibility values were normalized by the sample masses.

2.5. X-ray absorption spectroscopy

Both unheated and heated bulk soil samples were analyzed for Fe K-edge XAS. Spectra were collected at the XAFS beamline at Elettra Sincrotrone (Trieste, Italy) (Aquilanti et al., 2017). Powdered soil samples (~50 mg) were pressed into pellets with the addition of PVP, sealed with Kapton tape and mounted onto a sample holder at RT. Spectra were collected in transmission mode, accounting for beam attenuation as a function of incoming photon energy (Mobilio, 2015) using a Si (1 1 1) monochromator calibrated to the first-derivative maximum of the K-edge absorption spectrum of metallic Fe foil (7112 eV). The foil was continuously monitored to account for small energy shifts during sample measurements. Higher harmonics in the beam were eliminated by detuning the monochromator by 30 % of its maximal intensity. Multiple (3) scans per sample were acquired from 6817 to 7661 eV, at a speed of 1.5 eV s^{-1}.

X-ray absorption near-edge spectroscopy (XANES) and Extended X-ray absorption fine-structure (EXAFS) were targeted. Data processing (i.e., reference alignment, background subtraction, normalization, deglitching and spectra merging) was performed using the Athena software (Ravel and Newville, 2005).

The contribution of different Fe species was assessed by comparing our spectra with atomic structures of reference Fe-bearing compounds (O'Day et al., 2004) (Figure S2). Linear combination fitting (LCF) was performed both in the XANES and EXAFS region without constraining the sum of the fitted fractions to reach 100 %, as done in Giannetta et al. (2020). We focused on the −20 to 40 μ(E) energy range for XANES and on the 2.5——12 $Å^{-1}$ range for the EXAFS region (k^3-weighted spectra).

2.6. Statistical analyses

RStudio (R version 4.0.2) was used for the statistical analyses. Before making group comparisons, Shapiro-Wilk's and Levene's tests were used to inspect the normality and homoscedasticity of the data, respectively. Two different linear models were applied: one-way ANOVA was used to compare the whole set of samples according to a single factor, while linear mixed models (LMM) were used to test the role of selected categorical variables along the T-kinetic (with T being the second level of comparison). Autocorrelation, where present, was considered within the model itself. Correlation coefficients were extracted from the correlation matrixes computed by Pearson parametric method.

We opted for a conservative approach in the evaluation of the XAS spectra, avoiding an expert-driven choice of the best LCF output. We kept the top fits (10 per each sample at each temperature in each region, i.e., XANES and EXAFS) obtained by the LCF procedure. The results were projected onto score plots (Principal Component Analysis) and clustered (Ward's agglomeration method). Then, the outputs that maximized multiple fitting parameters (Chi-squared, AIC, Relative Likelihood and Final Prediction Error), and that recurred with consistency alongside the T-kinetic, were selected (detailed description of the procedure in Supporting Information, Figures S3-S5, Table S4). The abundance of Fe reference compounds was calculated by averaging the abundance within the chosen cluster, separately for each T. Fe species abundances were then normalized to reach 100 %.

3. Results and discussion

3.1. Fe pools and crystalline degree

Increasing Ts did not induce any differences in Fe_{DCB} contents ($p > 0.05$, Table 1), which were generally higher in BEECH with respect to PINE samples ($p < 0.05$). Higher Fe_{OXA} values were detected with increasing Ts, with a statistically significant trend only in the BEECH series ($p < 0.05$). The Fe_{OXA}:Fe_{DCB} ratio is widely employed as an indicator of phase crystallinity, with lower values in case of more ordered forms (Hall et al., 2018). In our case, at RT, poorly ordered Fe phases contributed to ca. 17 % of the total pedogenic Fe oxides. These values are in line with the scarce development degree expected in alpine soils, and the inhibitory effects of OM on oxide crystallization (Borggaard, 1985).

Although a slight increase in this ratio upon increasing Ts was visible in several samples, no significant changes were observed ($p > 0.05$, Table 1), suggesting that heating at 200 and 300 °C is not sufficient to alter oxide crystallinity. This is in line with some of the results by Jordanova et al (2018) and consistent with existing studies, that detected the presence of highly crystalline Fe oxides only with Ts as high as 600–900 °C (Bora et al., 2012; Dionísio et al., 2009).

A decrease in organo-mineral complexes was observed upon increasing Ts, in agreement with existing studies (Norouzi and Ramezanpour, 2013). The T-related downtrend in Fe_{PYRO}:Fe_{DCB} was more pronounced and significant only in the BEECH subset ($p < 0.05$), possibly due to a lower thermal stability beech-derived organic moieties.

Soil specimens were characterized by multiple phases (FE-SEM images at 4 k magnification in Figure S6). Structures rich in Fe and O were detected (through elemental maps in Fig. 1), corroborating the presence of Fe oxides. The Fe phases occurred in the shape of husks (Fig. 1a and 1b, zoom 1), disordered spherical features (Fig. 1d, zoom 2), rods (Fig. 1d, zoom 3). The Fe oxides often coated other mineral particles (Fig. 1c and 1d) and, infrequently, they appeared as isolated spherical structures (Fig. 1e and 1f). These latter shapes likely derived from a heat-induced synthesis process leading to the minimization of surface energy (Bora et al., 2012). Analogous, although smaller, C-rich Fe oxides

Table 1
DCB, OXA and PYRO extractable Fe in the soil samples at 25, 200 and 300 °C.

Sample	T (°C)	Fe_{DCB} (g kg^{-1})	Fe_{OXA} (g kg^{-1})	Fe_{PYRO} (g kg^{-1})	Fe_{OXA}: Fe_{DCB} (%)	Fe_{PYRO}: Fe_{DCB} (%)
BE1	25	16.5	3.2	3.0	19.4	18.2
	200	17.5	3.3	2.6	18.9	14.9
	300	18.7	4.1	1.1	21.9	5.9
BE2	25	16.6	2.6	1.6	15.7	9.6
	200	16.8	4.9	1.2	29.2	7.1
	300	17.1	4.9	0.7	28.7	4.1
BE3	25	19.4	1.9	0.7	9.8	3.6
	200	20.0	2.7	0.6	13.5	3.0
	300	20.9	2.9	0.5	13.9	2.4
BE4	25	13.8	2.1	0.9	15.2	6.5
	200	13.7	2.3	0.7	16.8	5.1
	300	13.9	3.0	0.4	21.6	2.9
BE5	25	16.4	2.3	1.0	14.0	6.1
	200	15.5	2.3	0.9	14.8	5.8
	300	16.7	2.7	0.4	16.2	2.4
BE6	25	17.8	1.3	0.7	7.3	3.9
	200	17.5	1.4	0.6	8.0	3.4
	300	21.4	1.7	0.3	7.9	1.4
BE7	25	21.0	1.5	1.3	7.1	6.2
	200	21.1	1.4	0.9	6.6	4.3
	300	24.4	1.7	0.4	7.0	1.6
BE8	25	18.3	3.0	1.4	16.4	7.7
	200	19.6	3.8	1.1	19.4	5.6
	300	21.7	3.8	0.7	17.5	3.2
BE9	25	19.0	2.1	1.3	11.1	6.8
	200	19.5	4.8	1.1	24.6	5.6
	300	23.3	3.5	0.8	15.0	3.4
BE10	25	9.7	1.3	0.8	13.4	8.2
	200	8.7	1.6	0.7	18.4	8.0
	300	9.6	1.8	0.5	18.8	5.2
PI1	25	25.6	1.4	2.3	5.5	9.0
	200	20.8	2.0	0.9	9.6	4.3
	300	21.8	2.4	0.9	11.0	4.1
PI2	25	9.7	1.7	0.7	17.5	7.2
	200	9.8	1.3	0.7	13.3	7.1
	300	10.1	1.7	0.5	16.8	5.0
PI3	25	12.9	3.1	1.3	24.0	10.1
	200	12.5	2.4	1.2	19.2	9.6
	300	14.5	3.4	1.1	23.4	7.6
PI4	25	18.2	4.0	2.0	22.0	11.0
	200	18.6	4.1	1.5	22.0	8.1
	300	19.8	5.0	0.7	25.3	3.5
PI5	25	10.0	2.5	1.1	25.0	11.0
	200	10.4	3.9	1.1	37.5	10.6
	300	10.5	2.9	0.9	27.6	8.6
PI6	25	9.6	3.2	0.7	33.3	7.3
	200	9.2	3.4	0.9	37.0	9.8
	300	10.0	3.3	0.8	33.0	8.0
PI7	25	9.1	3.6	1.2	39.6	13.2
	200	8.9	3.9	1.2	43.8	13.5
	300	9.9	3.8	1.0	38.4	10.1
PI8	25	9.5	1.6	0.2	16.8	2.1
	200	9.4	1.4	0.2	14.9	2.1
	300	10.1	2.1	0.3	20.8	3.0

spherules have also been observed in soils affected by natural fires (Jordanova et al., 2019).

3.2. Identification of Fe oxides and magnetic properties

As expected from the site selection, the soils differed in starting mineralogical composition, with chlorite, serpentine, amphiboles and micas identified among the major silicate minerals (Figure S7). At room temperature (RT), goethite was not detected in the XRD patterns (Fig. 2, green spectra). No peaks were visible at the highest intensity reflection of goethite (0.418 nm), and only a weak reflection at 0.245 nm was observed (where quartz might yet be interfering). Small amounts of ferrihydrite were present in BE4 and PI7 (broad reflection at 0.224 nm), both developed on schist. Either maghemite or magnetite was evident in BE4, BE10, and PI5 (reflection at 0.251–0.253 nm), with a stronger signal in the latter than in the other samples.

Higher Ts induced only small variations in reflections attributed to Fe oxides (Fig. 2, orange and brown spectra). At 300 °C, a minor increase in maghemite or magnetite was detected in sample BE10 (developed on serpentine, with high OC contents) by the peak at 0.251 nm (with a possible coexistence of hematite), and hematite was detected in sample PI5 (developed on serpentine, with high OC contents) by the reflection at 0.269 nm. The tested Ts did not cause a complete transition to more crystalline Fe species (no sharper reflections), as already suggested by the results of the chemical extractions.

The abundance of ferromagnetic minerals in samples BE4 and PI5 was detected by low-T remanence measurements. The hump at 120 °K in Fig. 3a and 3b represents the Verwey transition (highlighted by the blue arrows), and is characteristic of magnetite. At RT (green curves to the left), the Verwey transition was more prominent in sample PI5 (Fig. 3b) than in BE4 (Fig. 3a). This finding points to a greater presence of magnetite in sample PI5, developed on serpentine. The slightly suppressed Verwey transition of BE4 (Fig. 3a) likely indicates partially oxidized magnetite, or the co-existence with maghemite. Also, sample BE4 displayed higher field-cooling (FC) than zero-field-cooling (ZFC) values (Fig. 3a). This behavior is a symptom of the greater proportion of multi-domain, coarser-grained magnetite particles (Carter-Stiglitz et al., 2006). Since PI5 exhibited the opposite feature (higher ZFC than FC values, Fig. 3b), an abundance of single-domain size magnetite particles can be hypothesized. At 300 °C (brown curves to the right), the prominence of the Verwey transition (blue arrow) increased in sample PI5 (Fig. 3b), pointing to a greater contribution of magnetite at high T.

The saturation magnetization (M_S) values were notably higher in PI5 with respect to the other samples (Fig. 3c), pointing to a greater concentration of magnetic minerals (Liu et al., 2012). This agrees with the peak representing either maghemite or magnetite in the XRD spectra of PI5 (Fig. 2), and may reflect the presence of lithogenic magnetite in the serpentinite soil parent material.

Hysteresis parameters in the range observed here (M_R:M_S < 0.1, H_C > 5mT, Fig. 3d) are characteristic of superparamagnetic particles mixed with single-domain grains (Till et al., 2010). No unequivocal increase in H_C and M_R:M_S values emerged that would suggest growth of nanoparticles upon higher T (PI7 shifted towards lower values, and an opposite trend was displayed by BE10). The duality in particle-size transitions (moderate in entity) is not totally unexpected. Pyrogenic ferromagnetic phases have been documented to be finer-grained than typical pedogenic mineral assemblages (Oldfield and Crowther, 2007; Schwertmann, 1988), while Ts close to 300 °C are known to promote particle aggregation, with an increase in the size distribution and a modification of particle morphology (Redl et al., 2004). There was little observable difference in low-T susceptibility for heated and unheated samples of BE4 (Figure S8).

XANES data indicated the occurrence of chlorite, smectite and, occasionally, goethite (Table 2), with hardly any difference in Fe speciation for unheated *vs.* heated samples. The contribution of other compounds, like Fe(III)-citrate, was minimal. Chlorite and smectite were the most abundant. The Fe-rich chlorite signal detected in the diffraction patterns (Figure S7, Table S5) agrees with the spectroscopic analysis, while the presence of smectite in these soils (not visible in the XRD spectra of bulk samples) was previously documented (Bonifacio et al., 2010).

EXAFS proved to be more sensitive to Fe(III)-citrate and oxides rather than Fe-bearing phyllosilicates (Table 2). Given the highly different magnetic signatures of the soils (Fig. 3), we expected a diversity in starting Fe species composition. Still, maghemite was identified as the dominant Fe oxide (with a rather homogeneous content in the samples) and, as XRD showed the reflections characteristics of either magnetite or maghemite in three out of four cases (BE4, BE10, PI5), it is reasonable to hypothesize a varying degree of magnetic mineral oxidation.

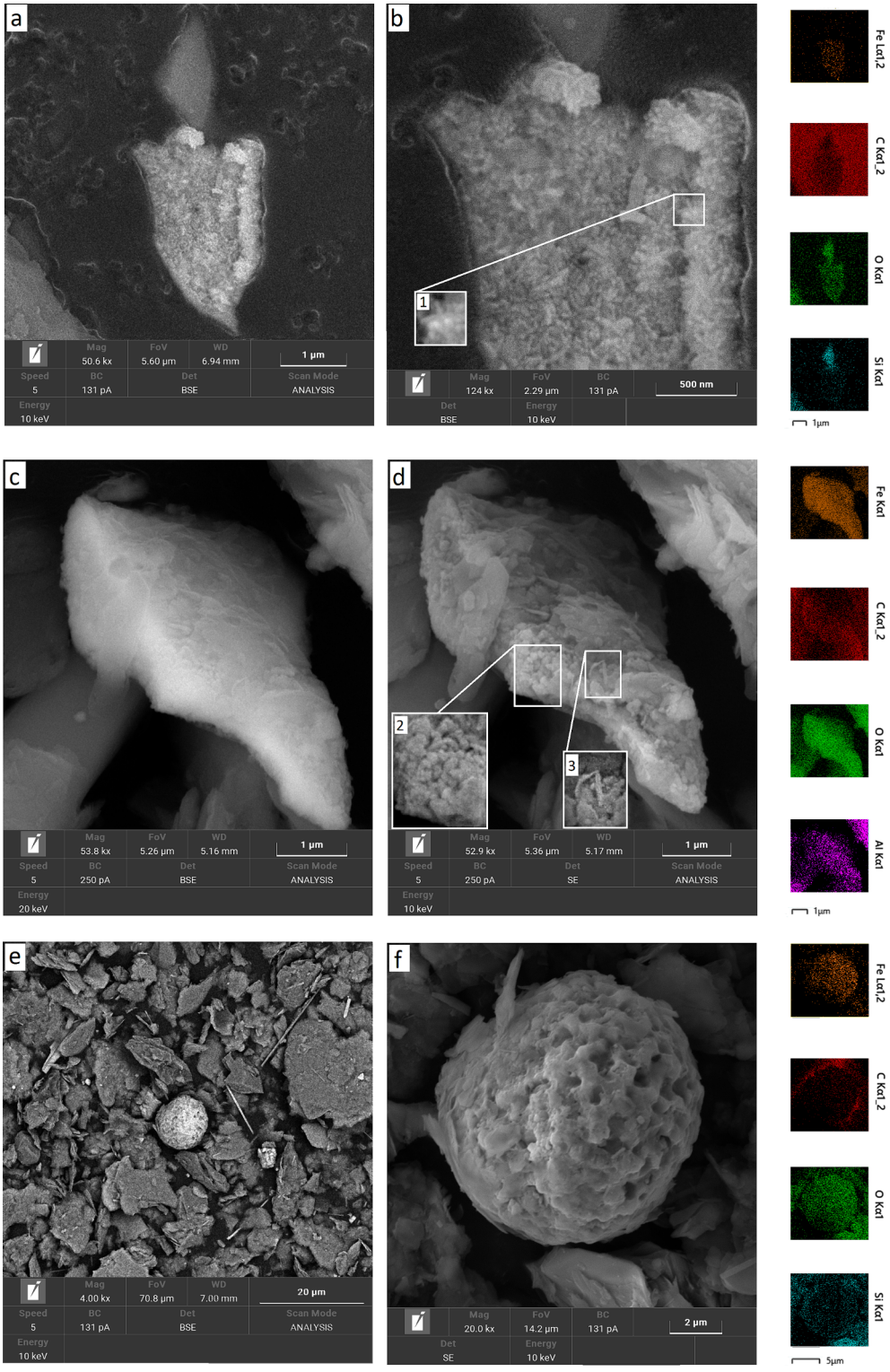

Fig. 1. FE-SEM images collected for a) and b) sample PI7 (soil on schist, PINE vegetation) at 200 °C (upper panel); c) and d) sample BE4 (soil on schist, BEECH vegetation) at 200 °C (middle panel); e) and f) sample PI7 at 300 °C (lower panel). Elemental maps and zooms on selected morphological details (1, 2, 3) are displayed.

3.3. Thermal transformation of Fe species

The occurrence of oxidative processes was evidenced by the appearance of hematite in samples BE4 and PI5 (more than 5 % of hematite at 300 °C, EXAFS data in Table 2). These contents are relatively low and close to the detection limit of the instrument, but the tendency in increasing values is well expressed and consistent in both samples. We hypothesize involvement of organo-mineral complexes in hematite formation, as EXAFS exhibited decreasing Fe(III)-citrate abundance with increasing Ts (in BE4, PI5 and PI7, Table 2), and also the Fe_{PYRO}:Fe_{DCB} ratio decreased (Table 1). This T-induced trend was more marked in the wet chemistry results than in EXAFS, possibly because inner-sphere

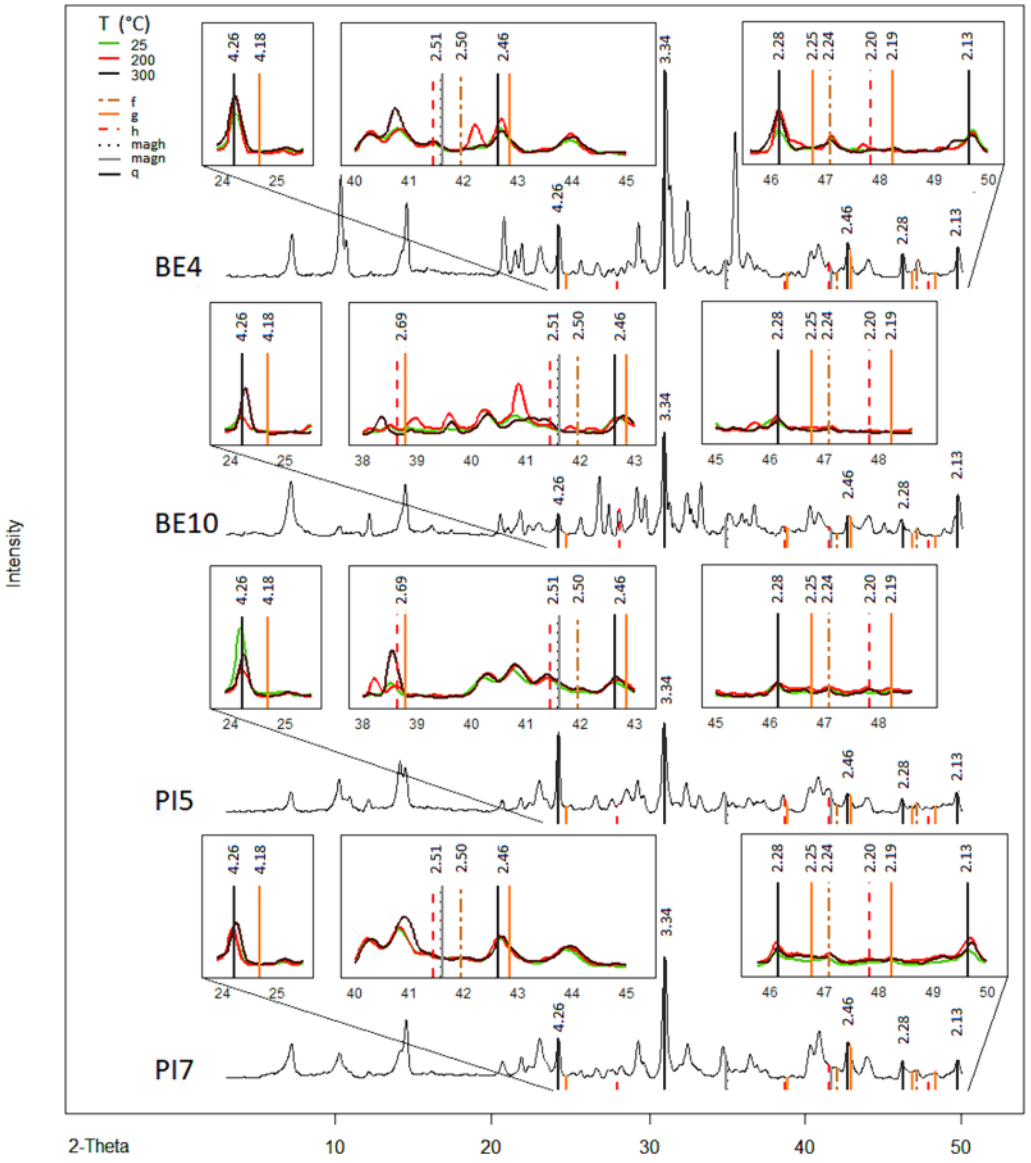

Fig. 2. Complete XRD spectra of the selected samples (BE4 and PI7 developed on schist, while BE10 and PI5 developed on serpentine) in black solid line, with panels focusing on selected regions. Colour code assigned according to sample T (green: 25 °C, orange: 200 °C, brown: 300 °C). Vertical lines correspond to characteristic reflections, in Å, of ferrihydrite (f), goethite (g), hematite (h), maghemite (magh), magnetite (magn) and quartz (q).

complexes within mineral particles mask the signal of outer-sphere surface ones (Martínez et al., 2006). The decomposition of Fe(III)-citrate at 460 °C in air has been documented to yield hematite formation (Srivastava et al., 1985), while lower Ts (280 °C) can originate a mixture of hematite and maghemite (Bassi et al., 1984). The breakage of the Fe(III)-citrate C = O bonds liberates Fe atoms, that may subsequently serve as precursors for hematite formation (Ou et al., 2008). Partial conversion of maghemite into hematite cannot be excluded. This structural T-driven inversion, involving the (*111*) and (*100*) axes of maghemite and (*001*) and (*100*) of hematite (Bora et al., 2012), results in a mineral species with a lower enthalpy under aerobic surface conditions (Johnston et al., 2019).

Hematite was not observed in low-T remanence measurements of heated/unheated BE4 and PI5 (no Morin transition, hump at 260 °K in Fig. 3a and 3b). The lack of this trait could be ascribed to vacancies and impurities or, alternatively, could be due to the presence of very small particles (Coey, 1988) (plausible, as derived by the squareness plot, Fig. 3d). The presence of small hematite particles is consistent with the increase in Fe_{OXA} upon heating, as fine grained oxides, albeit crystalline, are more sensitive to this chemical extraction (Lanzl et al., 2012).

The transitional nature of maghemite and the T corresponding to its full hematite conversion are still debated, as this process is highly dependent on grain size and impurities (Till et al., 2021). The crystalline degree of maghemite, which is usually poor at these Ts (Jeleńska et al., 2010), would agree with the unaltered Fe_{OXA}:Fe_{DCB} ratio observed upon soil heating (Table 1). This mineral assumes prismatic features over 600 °C (Bora et al., 2012), remaining in the form of husk-like structures up to 250 °C (Sayed and Polshettiwar, 2015). We witnessed the presence of Fe-rich particles composed of superimposed husks in PI7 (Fig. 1b, zoom 1), so it is likely that those crystals comprised maghemite formations maintaining such a shape up to 200 °C. Superparamagnetic and single-domain maghemite particles have been also observed in the uppermost horizons of fire-affected soils (Jordanova et al.,2018), where they were responsible for an increase in the soil magnetic signal. The same enhancement in single-domain magnetic particles was observed in our sample PI5 at high T (Fig. 3b). XANES also evidenced the presence of goethite in samples BE4 and PI5 (Table 2). We did not detect this mineral in the XRD spectra (Fig. 2). Still, as goethite has often been observed

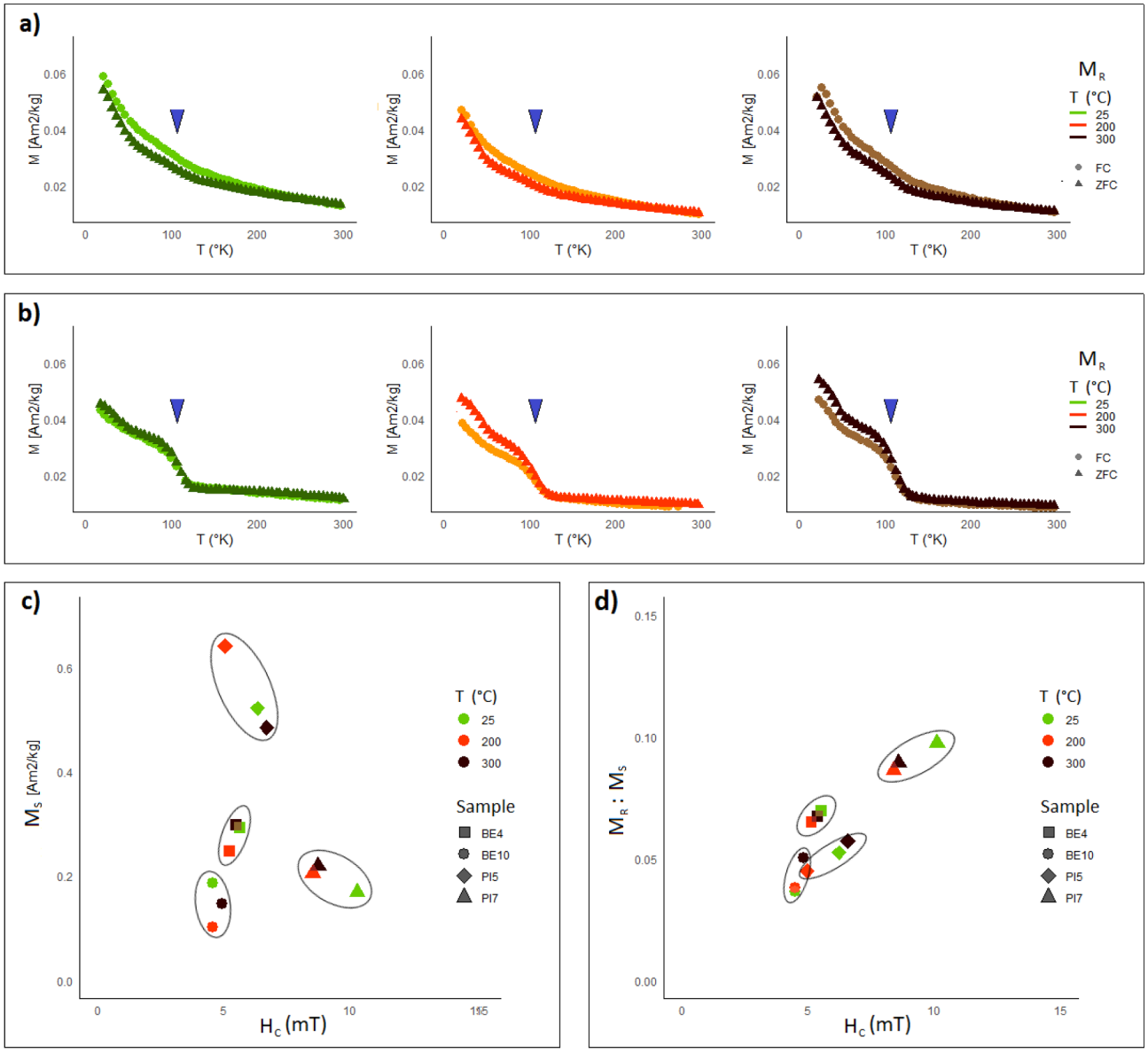

Fig. 3. Low-T remanence measurements after field-cooling (FC) and zero-field cooling (ZFC) of a) sample BE4 (soil on schist, BEECH vegetation) at 25–200-300 °C; b) sample PI5 (soil on serpentine, PINE vegetation) at 25–200-300 °C, with blue arrow indicating the Verwey transition; c) saturation magnetization measurements *vs.* H_C; d) hysteresis squareness plot (M_R:M_S *vs.* H_C). Colour code is assigned according to T (green: 25 °C, orange: 200 °C, brown: 300 °C). In figures c) and d),samples are identified by the marker shape, and enclosed in an ellipse.

as nano-rods (Penn et al., 2006) and lath-shaped crystals in soils heated at 250–300 °C (Dionísio et al., 2009), hints to its presence can be derived from the shape of the Fe-structures in the SEM image of sample BE4 (Fig. 1d, zoom 3). We are then prone to hypothesize that conversion of goethite into hematite also presumably occurred. This transformation, attributed to the well documented dehydroxylation reaction (Schwertmann and Fechter, 1984), usually begins at 150 °C in isolated minerals (Cudennec and Lecerf, 2005) and was previously observed at 250 °C in heated soils (Dionísio et al., 2009). Mild-T conversion of goethite into hematite would produce a highly disordered mineral structure, with excessive OH^- and Fe-deficiency, rich in nano-pores due to shrinking occurring during dehydration (Gualtieri and Venturelli, 1999). Thus, proto-hematite formation seems a plausible result of the heating treatment in our soils, and the poor crystalline degree of this mineral would also explain the lack of decreasing Fe_{OXA}:Fe_{DCB} values (that would mirror an increase in crystalline order) for greater heat intensities (Table 1). Presence of Al-substituted hematite, with small crystals (Brown, 1980), is a possible explanation for the lack of variations in the Fe_{OXA}:Fe_{DCB} ratio. However, these soils were collected on the same geological formation where Al-poor serpentinite is present, if not dominating (Bonifacio et al., 2013).

3.4. *Organo-mineral association – Interactions and affinity*

Since one of the samples (PI5) displayed a greater concentration of magnetic minerals at 300 °C (hump in Fig. 3b), an increase in maghemite or magnetite contents occurred. The formation of pure magnetite has to be excluded: XAS did not detect magnetite and no clear decreasing trend in coercitivity values could be observed with increasing Ts (Fig. 3c and 3d). We could rather ascribe the oscillating coercitivity values to the presence of maghemite along with magnetite, as this behavior was previously reported by Evans and Heller (2003) in the presence of intergrowth of partially oxidized titanomagnetite and by Redl et al. (2004) when magnetite seeds were added to iron nano-phases.

Table 2
Fe species percentages as obtained by LCF after the clustering procedure, operated separately in the XANES and in the EXAFS region. Data have been normalized to reach 100 %. Reference compounds: chlorite (Ch.), Fe(III)-citrate (Citr.), ferrihydrite (F.), goethite (G.), hematite (H.), maghemite (Magh.), magnetite (Magn.) and smectite (Sm.).

Region	ID	T (°C)	Ch.	Citr.	F.	G.	H.	Magh.	Magn.	Sm.
XANES	BE4	25	45			2				53
		200	47	1		2				50
		300	48	1		1				50
	BE10	25	34							66
		200	38	1		2				59
		300	42							58
	PI5	25	52			4				44
		200	52	1		2				45
		300	48			2				50
	PI7	25	80							20
		200	77							23
		300	78							22
EXAFS	BE4	25	34	33			1	32		
		200	36	30			2	32		
		300	35	28			5	32		
	BE10	25	34	29				33		4
		200	37	32				26		5
		300	39	29				30		2
	PI5	25	42	31			1	26		
		200	42	29			3	26		
		300	41	27			6	26		
	PI7	25	50	13	1			25		11
		200	52	13				27		8
		300	55	5		1		29		10

Magnetite formation is favored by anoxic conditions (Skinner and Fitzpatrick, 1992), therefore reducing conditions were plausibly established within the soil matrix at high T in sample PI5. This occurred in dependance of two factors: soil OC content and OM composition. Sample PI5 presented high amounts of OC, more than twice than BE4 (Table S2). Therefore, the electron-donor potential of OM in this sample was amplified. Compounds derived from coniferous vegetation are then known to release considerable amounts of pyrolysis by-products, like carbon monoxide and other reduced gases (Liu et al., 2017). Their potential as electron transfers to Fe species has been verified (Jozwiak et al., 2007) even in the case of soil heating experiments performed in air (Johnston et al., 2019). This feature might concur in explaining the high-T magnetic mineral enrichment in sample PI5 (developed under conifer canopy cover), which did not occur for BE4 (due to less OM and more labile compounds).

With Ts > 200 °C, a systematic decrease in OC and an increase in soil pH were observed in our previous investigation (Negri et al., 2021), as shown in Table S2. The OC_{PYRO}, conversely to Fe_{PYRO}:Fe_{DCB}, did not display a systematic decrease with increasing T (Table S6), and this might be explained - as above mentioned - by the fact that the PYRO solution is not strictly selective for the extraction of Fe-bound OM (Kögel-Knabner et al., 2008).

The OC_{PYRO}:OC contents at RT (Fig. 4a) are in line with values reported for soils developed under forest canopy cover (Ohno et al., 2017), and a relative enrichment in the PYRO-dispersible OM pool emerged at the highest tested T. The anticorrelation between OC_{PYRO}:OC *vs.* OC ($R = -0.651$, $p < 0.001$) occurred in parallel with a relatively weak and yet significant positive relationship between OC_{PYRO}:OC and pH in PINE samples ($R = 0.569$, $p < 0.01$). Decreasing E2:E3 values of PYRO-extracted OM were detected for PINE samples at greater Ts (Fig. 4b), a downtrend that mirrors a slight increase in molecular size of the extracted OM, consistent with the heat-induced formation of large polycondensed compounds (Knicker, 2011). Trends in PYRO-extracted OM SUVA were the opposite in the two datasets (BEECH *vs*. PINE, Fig. 4c). The highest recorded values, for PINE at 300 °C, express the great aromatic character of the isolated OM, as expected from the thermal alteration of its starting OM composition (Knicker, 2011; Negri et al., 2021). The PINE subset exhibited the presence of large aromatic compounds at high-T (slight but significant anticorrelation between SUVA *vs*. E2:E3; $R = -0.512$, $p < 0.05$), while more labile compounds emerged in BEECH for increasing Ts (anticorrelation OC_{PYRO}:OC *vs*. SUVA, $R = -0.522$, $p < 0.001$).

Regarding OM stabilization dynamics, a greater mineral-bound OM fraction (the non-dispersible pool) was found in PINE rather than in BEECH samples ($p < 0.01$, Fig. 4a). This could be ascribed to a strikingly different OM composition, resulting in the preferential association of large aromatic compounds with Fe oxides (Chassé et al., 2015; Ohno et al., 2017). Still, at 300 °C we observed a higher fraction of dispersible OM in both the subsets. This suggests that, despite the abundance of aromatic compounds at least in heated PINE samples (Fig. 4c), OM adhesion to mineral surfaces was not favored by high Ts.

On this point, we should consider that large organic clods and bulky OM agglomerations are known to be more easily extractable (because of a less intimate adhesion) (Kaiser and Guggenberger, 2007). Also, the abrupt increase in pH caused by OM combustion and the consequent increase in the negative surface charge of most soil mineral particles (Diehl et al., 2010) may have favoured a more pronounced electrostatic repulsion (Mayer and Xing, 2001), eventually leading to weaker organo-mineral associations. Thus, the structural heat-induced changes borne by mineral phases (synthesis of defect-rich Fe forms) and OM (enrichment in condensed and aromatic compounds, at least for PINE samples) could have potentially promoted the stabilization of the remaining OM. Nonetheless, OM was observed to be highly dispersible at the high pH values resulting at 300 °C, such that thermally altered OC might be weakly retained on mineral phases in an after-fire natural scenario.

4. Conclusions

If we place these findings in the context of natural ecosystems, we deem the thermal evolution of soil Fe species to be primarily directed towards oxidative processes. The onset for reducing conditions seems to be provided only by abundant OC loads (higher than 30 g kg^{-1}), especially if coupled with an aromatic character. This would explain why a significant increase in surface magnetism was detected in conifer-dominated forest soils after wildfire occurrence.

In alpine soils, Ts up to 300 °C seem to hinder the formation of Fe

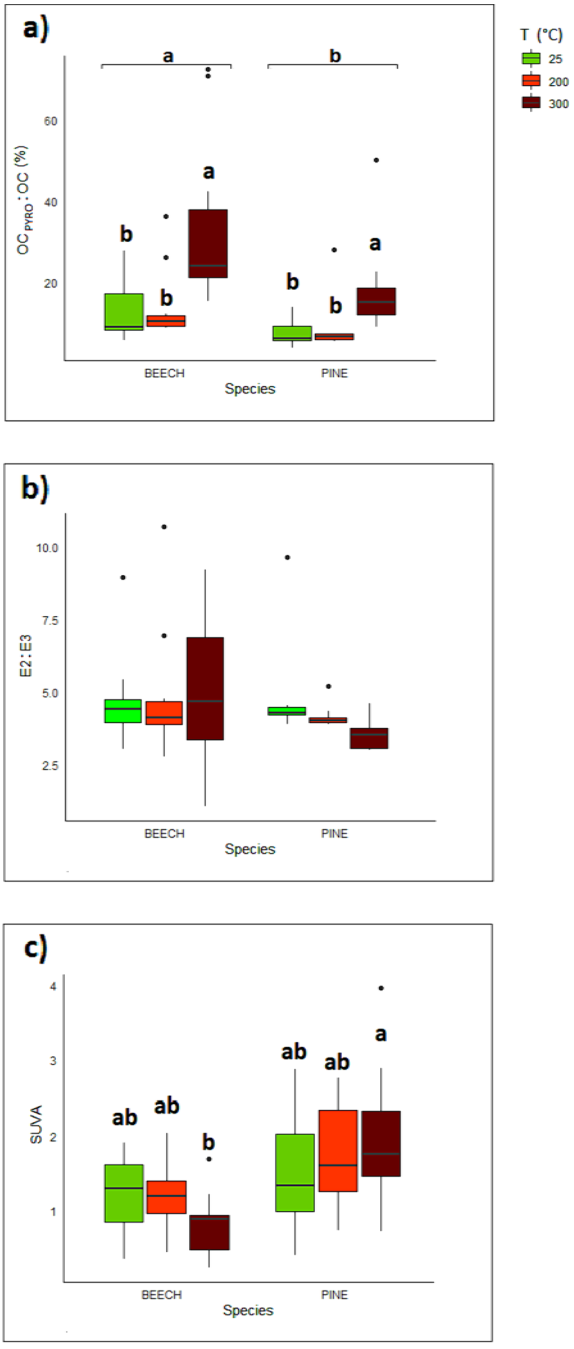

Fig. 4. Boxplots depicting a) OC_{PYRO}:OC (%), b) E2:E3 and c) SUVA of the PYRO extraction. Colour code assigned according to T (green: 25 °C, orange: 200 °C, brown: 300 °C), letters assigned according to statistically significant differences in mean values.

species with a greater crystalline order, notwithstanding the pre-existing differences in native Fe forms and soil OM. Crystalline Fe oxides are known to show a higher affinity for OM than poorly ordered Fe phases which are nonetheless able to provide stabilization for a substantial amount of OM due to their high surface area and reactivity. At 300 °C, the conversion of soil Fe species and OM resulted in weak organo-mineral associations, underlining that even moderate heating treatments are sufficient to considerably impact OC dynamics (OM oxidation aside), affecting alpine ecosystems as a whole.

Modifications in fire regimes are on the rise, and the study of the thermal evolution of Fe phases (and association with OM) should be emphasized, especially considering that soils developing in different biomes might not unequivocally respond to a fire-induced heating treatment.

Funding Sources

This work was funded by the University of Torino in the framework of the project *Alterations of soil physico-chemical properties as a consequence of forest fires* (UNITO S1921 EX-POST).

CRediT authorship contribution statement

Sara Negri: Conceptualization, Data curation, Formal analysis, Investigation, Methodology, Software, Validation, Visualization, Writing – original draft, Writing – review & editing. **Beatrice Giannetta:** Data curation, Formal analysis, Methodology, Supervision, Writing – review & editing. **Jessica Till:** Formal analysis, Investigation, Supervision, Writing – review & editing. **Danilo Oliveira de Souza:** Data curation, Methodology, Supervision, Writing – review & editing. **Daniel Said-Pullicino:** Conceptualization, Supervision, Validation, Writing – review & editing. **Eleonora Bonifacio:** Conceptualization, Funding acquisition, Project administration, Resources, Supervision, Writing – review & editing.

Declaration of competing interest

The authors declare the following financial interests/personal relationships which may be considered as potential competing interests: Geoderma editor-in-chief - D.S.P. Geoderma editorial advisory board - E. B.

Data availability

Data will be made available on request.

Acknowledgments

We thank Maria Carmen Valsania for having given support and guidance during microscopy analyses. We acknowledge ELETTRA for the provision of synchrotron radiation facilities and thank Giuliana Aquilanti and Luca Olivi (ELETTRA, XAFS beamline) for their support during the synchrotron measurements (proposal 20200417). We thank Peggy O'Day (University of California Merced) and all the co-authors of the O'Day et al. (2004) paper for providing the spectra of the standards used for the LCF. We wish to thank the four anonymous reviewers who thoroughly revised the manuscript. Following their suggestions, several improvements were included.

Appendix A. Supplementary data

Supplementary data to this article can be found online at https://doi.org/10.1016/j.geoderma.2024.116858.

References

Aquilanti, G., Giorgetti, M., Dominko, R., Stievano, L., Arčon, I., Novello, N., Olivi, L., 2017. Operando characterization of batteries using x-ray absorption spectroscopy: advances at the beamline XAFS at synchrotron Elettra. J. Phys. D Appl. Phys. 50, 74001.

Araya, S.N., Meding, M., Berhe, A.A., 2016. Thermal alteration of soil physico-chemical properties: a systematic study to infer response of Sierra Nevada climosequence soils to forest fires. Soil 2, 351–366.

Araya, S.N., Fogel, M.L., Berhe, A.A., 2017. Thermal alteration of soil organic matter properties: a systematic study to infer response of Sierra Nevada climosequence soils to forest fires. Soil 3, 31.

Badía-Villas, D., González-Pérez, J.A., Aznar, J.M., Arjona-Gracia, B., Martí-Dalmau, C., 2014. Changes in water repellency, aggregation and organic matter of a mollic horizon burned in laboratory: soil depth affected by fire. Geoderma 213, 400–407.

Bassi, P.S., Randhawa, B.S., Jamwal, H.S., 1984. Mössbauer study of the thermal decomposition of iron (III) citrate pentahydrate. J. Therm. Anal. Calorim. 29, 439–444.
Bilardello, D., Jackson, M., 2013. What do the mumpsies do? IRM Q 11–15.
Bonifacio, E., Falsone, G., Piazza, S., 2010. Linking ni and cr concentrations to soil mineralogy: does it help to assess metal contamination when the natural background is high? J. Soil. Sediment. 10, 1475–1486.
Bonifacio, E., Falsone, G., Catoni, M., 2013. Influence of serpentine abundance on the vertical distribution of available elements in soils. Plant and Soil 368, 493–506.
Bora, D.K., Braun, A., Erat, S., Safonova, O., Graule, T., Constable, E.C., 2012. Evolution of structural properties of iron oxide nano particles during temperature treatment from 250 C–900 C: X-ray diffraction and fe K-shell pre-edge X-ray absorption study. Curr. Appl Phys. 12, 817–825.
Borggaard, O.K., 1985. Organic matter and silicon in relation to the crystallinity of soil iron oxides. Acta Agric. Scand. 35, 398–406.
Bowman, D.M.J.S., Balch, J.K., Artaxo, P., Bond, W.J., Carlson, J.M., Cochrane, M.A., D'Antonio, C.M., DeFries, R.S., Doyle, J.C., Harrison, S.P., et al., 2009. Fire in the Earth system. Science 324, 481–484.
Brown, G., 1980. Associated minerals, in: Brindley, G. W. & Brown, G. (Eds.) Crystal structures of clay minerals and their X-ray identification. London Mineralogical Society, pp. 361–410.
Buettner, S.W., Kramer, M.G., Chadwick, O.A., Thompson, A., 2014. Mobilization of colloidal carbon during iron reduction in basaltic soils. Geoderma 221, 139–145.
Burton, E.D., Choppala, G., Karimian, N., Johnston, S.G., 2019. A new pathway for hexavalent chromium formation in soil: fire-induced alteration of iron oxides. Environ. Pollut. 247, 618–625.
Carter-Stiglitz, B., Moskowitz, B., Solheid, P., Berquo, T.S., Jackson, M., Kosterov, A., 2006. Low-temperature magnetic behavior of multidomain titanomagnetites: TM0. TM16, and TM35, J geophys res: solid. Earth 111.
Certini, G., 2005. Effects of fire on properties of forest soils: a review. Oecologia 143, 1–10.
Chassé, A.W., Ohno, T., Higgins, S.R., Amirbahman, A., Yildirim, N., Parr, T.B., 2015. Chemical force spectroscopy evidence supporting the layer-by-layer model of organic matter binding to iron (oxy) hydroxide mineral surfaces. Environ. Sci. Tech. 49, 9733–9741.
Clement, B.M., Javier, J., Sah, J.P., Ross, M.S., 2011. The effects of wildfires on the magnetic properties of soils in the Everglades. Earth Surf. Proc. Land. 36, 460–466.
Coey, J.M.D., 1988. Magnetic properties of iron in soil iron oxides and clay minerals, in: Iron in Soils and Clay Minerals. Springer, pp. 397–466.
Cornell, R.M., Schwertmann, U., 2003. The iron oxides: structure, properties, reactions, occurrences and uses. John Wiley & Sons.
Cudennec, Y., Lecerf, A., 2005. Topotactic transformations of goethite and lepidocrocite into hematite and maghemite. Solid State Sci. 7, 520–529.
Czimczik, C.I., Masiello, C.A., 2007. Controls on black carbon storage in soils. Global Biogeochem. Cycles 21.
DeBano, L.F., Neary, D.G., Ffolliott, P.F., 1998. Fire effects on ecosystems. John Wiley & Sons, New York.
Diehl, D., Bayer, J.V., Woche, S.K., Bryant, R., Doerr, S.H., Schaumann, G.E., 2010. Reaction of soil water repellency to artificially induced changes in soil pH. Geoderma 158, 375–384.
Dionísio, A., Braga, M.A.S., Waerenborgh, J.C., 2009. Clay minerals and iron oxides-oxyhydroxides as fingerprints of firing effects in a limestone monument. Appl. Clay Sci. 42, 629–638.
Dong, C., 1999. PowderX: Windows-95-based program for powder X-ray diffraction data processing. J. Appl. Cryst. 32, 838.
Evans, M., Heller, F., 2003. Environmental magnetism: principles and applications of enviromagnetics. Elsevier.
Giannetta, B., Siebecker, M.G., Zaccone, C., Plaza, C., Rovira, P., Vischetti, C., Sparks, D. L., 2020. Iron (III) fate after complexation with soil organic matter in fine silt and clay fractions: an EXAFS spectroscopic approach. Soil Tillage Res. 200, 104617.
Gimeno-García, E., Andreu, V., Rubio, J.L., 2004. Spatial patterns of soil temperatures during experimental fires. Geoderma 118, 17–38.
Glasspool, I.J., Scott, A.C., Waltham, D., Pronina, N.V., Shao, L., 2015. The impact of fire on the late paleozoic Earth system. Front. Plant Sci. 6, 756.
Gualtieri, A.F., Venturelli, P., 1999. In situ study of the goethite-hematite phase transformation by real time synchrotron powder diffraction. Am. Mineral. 84, 895–904.
Hall, S.J., Berhe, A.A., Thompson, A., 2018. Order from disorder: do soil organic matter composition and turnover co-vary with iron phase crystallinity? Biogeochemistry 140, 93–110.
Jackson, M., Solheid, P., 2010. On the quantitative analysis and evaluation of magnetic hysteresis data. Geochemistry, Geophysics, Geosystems, p. 11.
Janzen, C., Tobin-Janzen, T., 2008. Microbial communities in fire-affected soils. Microbiology of Extreme Soils. Springer 299–316.
Jeleńska, M., Hasso-Agopsowicz, A., Kopcewicz, B., 2010. Thermally induced transformation of magnetic minerals in soil based on rock magnetic study and mössbauer analysis. Phys. Earth Planet. In. 179, 164–177.
Johnston, S.G., Karimian, N., Burton, E.D., 2019. Fire promotes arsenic mobilization and rapid arsenic (III) formation in soil via thermal alteration of arsenic-bearing iron oxides. Front. Earth Sci. 7, 139.
Jolly, W.M., Cochrane, M.A., Freeborn, P.H., Holden, Z.A., Brown, T.J., Williamson, G.J., Bowman, D.M.J.S., 2015. Climate-induced variations in global wildfire danger from 1979 to 2013. Nat. Commun. 6, 1–11.
Jordanova, D., Jordanova, N., Barrón, V., Petrov, P., 2018. The signs of past wildfires encoded in the magnetic properties of forest soils. Catena 171, 265–279.
Jordanova, N., Jordanova, D., Barrón, V., 2019. Wildfire severity: environmental effects revealed by soil magnetic properties. Land Degrad. Dev. 30, 2226–2242.
Jozwiak, W.K., Kaczmarek, E., Maniecki, T.P., Ignaczak, W., Maniukiewicz, W., 2007. Reduction behavior of iron oxides in hydrogen and carbon monoxide atmospheres. Appl. Catal. A 326, 17–27.
Kaiser, K., Guggenberger, G., 2007. Sorptive stabilization of organic matter by microporous goethite: sorption into small pores vs. surface complexation. Eur. J. Soil Sci. 58, 45–59.
Knicker, H., 2011. Pyrogenic organic matter in soil: its origin and occurrence, its chemistry and survival in soil environments. Quat. Int. 243, 251–263.
Kögel-Knabner, I., Guggenberger, G., Kleber, M., Kandeler, E., Kalbitz, K., Scheu, S., Eusterhues, K., Leinweber, P., 2008. Organo-mineral associations in temperate soils: integrating biology, mineralogy, and organic matter chemistry. J. Plant Nutr. Soil Sci. 171, 61–82.
LaGrow, A.P., Besenhard, M.O., Hodzic, A., Sergides, A., Bogart, L.K., Gavriilidis, A., Thanh, N.T.K., 2019. Unravelling the growth mechanism of the co-precipitation of iron oxide nanoparticles with the aid of synchrotron X-ray diffraction in solution. Nanoscale 11, 6620–6628.
Lanzl, C.A., Baltrusaitis, J., Cwiertny, D.M., 2012. Dissolution of hematite nanoparticle aggregates: influence of primary particle size, dissolution mechanism, and solution pH. Langmuir 28, 15797–15808.
Liu, W.-J., Li, W.-W., Jiang, H., Yu, H.-Q., 2017. Fates of chemical elements in biomass during its pyrolysis. Chem. Rev. 117, 6367–6398.
Liu, Q., Roberts, A.P., Larrasoaña, J.C., Banerjee, S.K., Guyodo, Y., Tauxe, L., Oldfield, F., 2012. Environmental magnetism: principles and applications. Rev. Geophys. 50.
Loeppert, R.H., I.w.p.,, 1996. Iron - methods of soil analysis, part 3: chemical methods. Madison, WI, USA.
Martínez, C.E., Bazilevskaya, K.A., Lanzirotti, A., 2006. Zinc coordination to multiple ligand atoms in organic-rich surface soils. Environ. Sci. Tech. 40, 5688–5695.
Mayer, L.M., Xing, B., 2001. Organic matter–surface area relationships in acid soils. Soil Sci. Soc. Am. J. 65, 250–258.
Mehra, O.P., Jackson, M.L., 1958. Iron oxide removal from soils and clays by a dithionite–citrate system buffered with sodium bicarbonate. Clays and Clay Minerals. Elsevier 317–327.
Merino, A., Fonturbel, M.T., Fernández, C., Chávez-Vergara, B., García-Oliva, F., Vega, J. A., 2018. Inferring changes in soil organic matter in post-wildfire soil burn severity levels in a temperate climate. Sci. Total Environ. 627, 622–632.
Mobilio, S., 2015. Introduction to matter radiation Interaction. Synchrotron Radiation. Springer 107–143.
Näthe, K., Levia, D.F., Steffens, M., Michalzik, B., 2017. Solid-state 13C NMR characterization of surface fire effects on the composition of organic matter in both soil and soil solution from a coniferous forest. Geoderma 305, 394–406.
Negri, S., Stanchi, S., Celi, L., Bonifacio, E., 2021. Simulating wildfires with lab-heating experiments: drivers and mechanisms of water repellency in alpine soils. Geoderma 402, 115357.
Norouzi, M., Ramezanpour, H., 2013. Effect of fire on chemical forms of iron and manganese in forest soils of Iran. Environ. Forensic 14, 169–177.
O'Day, P.A., Rivera Jr, N., Root, R., Carroll, S.A., 2004. X-ray absorption spectroscopic study of fe reference compounds for the analysis of natural sediments. Am. Mineral. 89, 572–585.
Ohno, T., Heckman, K.A., Plante, A.F., Fernandez, I.J., Parr, T.B., 2017. 14C mean residence time and its relationship with thermal stability and molecular composition of soil organic matter: a case study of deciduous and coniferous forest types. Geoderma 308, 1–8.
Oldfield, F., Crowther, J., 2007. Establishing fire incidence in temperate soils using magnetic measurements. Palaeogeogr. Palaeoclimatol. Palaeoecol. 249, 362–369.
Ou, X., Quan, X., Chen, S., Zhang, F., Zhao, Y., 2008. Photocatalytic reaction by fe (III)–citrate complex and its effect on the photodegradation of atrazine in aqueous solution. J. Photochem. Photobiol. A Chem. 197, 382–388.
Penn, R.L., Erbs, J.J., Gulliver, D.M., 2006. Controlled growth of alpha-FeOOH nanorods by exploiting-oriented aggregation. J. Cryst. Growth 293, 1–4.
Peuravuori, J., Pihlaja, K., 1997. Molecular size distribution and spectroscopic properties of aquatic humic substances. Anal. Chim. Acta 337, 133–149.
Ravel, B., Newville, M., 2005. ATHENA, ARTEMIS, HEPHAESTUS: data analysis for X-ray absorption spectroscopy using IFEFFIT. J. Synchrotron Radiat. 12, 537–541.
Redl, F.X., Black, C.T., Papaefthymiou, G.C., Sandstrom, R.L., Yin, M., Zeng, H., Murray, C.B., O'Brien, S.P., 2004. Magnetic, electronic, and structural characterization of nonstoichiometric iron oxides at the nanoscale. J. Am. Chem. Soc. 126, 14583–14599.
Reynard-Callanan, J.R., Pope, G.A., Gorring, M.L., Feng, H., 2010. Effects of high-intensity forest fires on soil clay mineralogy. Phys. Geogr. 31, 407–422.
Rita, A., Camarero, J.J., Nolè, A., Borghetti, M., Brunetti, M., Pergola, N., Serio, C., Vicente-Serrano, S.M., Tramutoli, V., Ripullone, F., 2020. The impact of drought spells on forests depends on site conditions: the case of 2017 summer heat wave in southern Europe. Glob. Chang. Biol. 26, 851–863.
Sayed, F.N., Polshettiwar, V., 2015. Facile and sustainable synthesis of shaped iron oxide nanoparticles: effect of iron precursor salts on the shapes of iron oxides. Sci. Rep. 5, 1–14.
Schwertmann, U., 1964. Differenzierung der eisenoxide des bodens durch photochemische extraktion mit saurer ammoniumoxalat-lösung. Zeischrift Für Pflanzenernährung, Düngung Und Bodenkunde 105–194.
Schwertmann, U., Fechter, H., 1984. The influence of aluminum on iron oxides: XI. aluminum-substituted maghemite in soils and its formation. Soil Sci. Soc. Am. J. 48, 1462–1463.
Schwertmann, U., 1988. Occurrence and formation of iron oxides in various pedoenvironments, in: Iron in Soils and Clay Minerals. Springer, pp. 267–308.

Servizio Geologico d'Italia, S.G., 2009. Carta geologica d'italia 1:50000. ISPRA e ARPA Piemonte.
Skinner, H.C.W., Fitzpatrick, R.W., 1992. Biomineralization. Catena Supplements 21, 432.
Smith, H.G., Sheridan, G.J., Lane, P.N.J., Nyman, P., Haydon, S., 2011. Wildfire effects on water quality in forest catchments: a review with implications for water supply. J. Hydrol. 396, 170–192.
Srivastava, A., Singh, P., Gunjikar, V.G., Sinha, A.P.B., 1985. Study of the thermal decomposition of iron and barium citrates. Thermochim Acta 86, 77–84.
Till, J.L., Jackson, M.J., Moskowitz, B.M., 2010. Remanence stability and magnetic fabric development in synthetic shear zones deformed at 500 C. Geochem. Geophys. Geosyst. 11.
Till, J.L., Moskowitz, B., Poulton, S.W., 2021. Magnetic properties of plant ashes and their influence on magnetic signatures of fire in soils. Front. Earth Sci. 8.
Till, J.L., Nowaczyk, N., 2018. Authigenic magnetite formation from goethite and hematite and chemical remanent magnetization acquisition. Geophys. J. Int. 213, 1818–1831.
Ulery, A.L., Graham, R.C., Bowen, L.H., 1996. Forest fire effects on soil phyllosilicates in California. Soil Sci. Soc. Am. J. 60, 309–315.
Varela, M.E., Benito, E., Keizer, J.J., 2010. Effects of wildfire and laboratory heating on soil aggregate stability of pine forests in Galicia: the role of lithology, soil organic matter content and water repellency. Catena 83, 127–134.
Wagai, R., Mayer, L.M., 2007. Sorptive stabilization of organic matter in soils by hydrous iron oxides. Geochim. Cosmochim. Acta 71, 25–35.
Weishaar, J.L., Aiken, G.R., Bergamaschi, B.A., Fram, M.S., Fujii, R., Mopper, K., 2003. Evaluation of specific ultraviolet absorbance as an indicator of the chemical composition and reactivity of dissolved organic carbon. Environ. Sci. Tech. 37, 4702–4708.
WRB, 2015. World Reference Base for soil resources 2014, update 2015. World Soil Resour. Rep.
Yang, F., Zhao, L., Gao, B., Xu, X., Cao, X., 2016. The interfacial behavior between biochar and soil minerals and its effect on biochar stability. Environ. Sci. Tech. 50, 2264–2271.